Advances in Nano Research, *Vol. 6 No. 4 (2018) 299-321*
DOI: https://doi.org/10.12989/anr.2018.6.4.299

A layerwise theory for buckling analysis of truncated conical shells reinforced by CNTs and carbon fibers integrated with piezoelectric layers in hygrothermal environment

Mohammad Hadi Hajmohammad [1], Mohammad Sharif Zarei [2], Ahmad Farrokhian [1] and Reza Kolahchi [*3]

[1] *Department of Mechanical Engineering, Imam Hossein University, Tehran, Iran*
[2] *Faculty of Engineering, Ayatollah Boroujerdi University, Boroujerd, Iran*
[3] *Department of Civil Engineering, Meymeh Branch, Islamic Azad University, Meymeh, Iran*

(*Received July 16, 2018, Revised October 3, 2018, Accepted October 8, 2018*)

Abstract. A layerwise shear deformation theory is applied in this paper for buckling analysis of piezoelectric truncated conical shell. The core is a multiphase nanocomposite reinforced by carbon nanotubes (CNTs) and carbon fibers. The top and bottom face sheets are piezoelectric subjected to 3D electric field and external voltage. The Halpin-Tsai model is used for obtaining the effective moisture and temperature dependent material properties of the core. The proposed layerwise theory is based on Mindlin's first-order shear deformation theory in each layer and results for a laminated truncated conical shell with three layers considering the continuity boundary condition. Applying energy method, the coupled motion equations are derived and analyzed using differential quadrature method (DQM) for different boundary conditions. The influences of some parameters such as boundary conditions, CNTs weight percent, cone semi vertex angle, geometrical parameters, moisture and temperature changes and external voltage are investigated on the buckling load of the smart structure. The results show that enhancing the CNTs weight percent, the buckling load increases. Furthermore, increasing the moisture and temperature changes decreases the buckling load.

Keywords: buckling; piezoelectric truncated conical shells; multiphase nanocomposite; layerwise theory; hygrothermal load

1. Introduction

The application of sandwich structures in many industries is rising due to their excellent properties such as high strength, low weight and resistance to fatigue. One of the special types of these structures is truncated conical shell with application in aerospace, marine and automobile industries. Due to their practical interest, sandwich structures have been the subject of numerous works. However, in this work, we focused on the buckling analysis of piezoelectric truncated conical shells.

Mechanical analysis of sandwich conical shells is reported by several researchers. Tong (1994) studied laminated conical shells using first order shear deformation theory (FSDT) based on power

*Corresponding author, Ph.D., Professor, E-mail: r.kolahchi@gmail.com

 ISSN: 2287-237X (Print), 2287-2388 (Online)

series solution. Sharnappa *et al*. (2007) presented the damping and frequency parameters of conical sandwich shell with electro-rheological fluid (ER) core. Free vibration of antisymmetric and symmetric cross-ply composite laminated truncated conical shells was studied by Viswanathan *et al*. (2012) using the spline function technique. Abediokhchi *et al*. (2013) investigated buckling of conical laminated shell panels using classical shell theory and solved using DQM. Based on improved higher-order panel theory, the buckling response of a sandwich truncated conical composite panel was performed by Malekzade Fard and Livani (2014). Nonlinear dynamics of laminated composite bimodular conical panels was presented by Khan and Patel (2015) by employing shooting technique coupled with length/pseudo-arc length continuation and Newmark time marching arc algorithms. Viswanathan *et al*. (2015) analyzed free vibration of anti-symmetric angle-ply laminated conical shells using Bickley-type splines to obtain the generalized eigenvalue problem. Buckling analysis of sandwich functionally graded conical panels was studied by Demir *et al*. (2016) using method of discrete singular convolution. An improved high-order theory was employed by Shekari *et al*. (2017) to present the vibration of sandwich truncated rotating conical shells with a soft core. Buckling vibration responses of sandwich laminated truncated conical shells were presented by Nasihatgozar and Khalili (2017) considering curvature effects. Sofiyev *et al*. (2017) demonstrated the effectiveness of functionally graded integrating for the vibration of truncated conical sandwich shells. The mechanical and thermal stability of a composite functionally graded truncated conical shell reinforced by carbon nanotube fibers were studied by Duc *et al*. (2017d).

For the published papers in the field of the piezoelectric sandwich structure, an efficient one-dimensional model was developed by Kapuria *et al*. (2003) for the statics of sandwich piezoelectric beams using third-order zigzag theory. An investigation on the nonlinear dynamic response and vibration of the imperfect laminated three-phase polymer nanocomposite panel resting on elastic foundations was presented by Duc *et al*. (2015). Coupled piezoelectric layerwise higher-order laminate mechanics were used by Plagianakos and Papadopoulos (2015), applicable to sandwich shells and shallow composite cylindrical under the electric and mechanical loads. Dynamic response of laminated sandwich plates with smart actuator and sensor layers and soft core were presented by Araújo *et al*. (2016) based on finite element model. Aylikci *et al*. (2017) studied the 3D buckling delamination problem in the PZT/Metal/PZT sandwich plates using the so-called 3D linearized theory of stability. Hajmohammad *et al*. (2017a) investigated dynamic buckling of viscoelastic laminated sandwich plate with CNT-reinforced layers and viscoelastic piezoelectric layers at the top and bottom face sheets. Kolahchi *et al*. (2017a) investigated wave propagation of smart viscoelastic nanocomposite sandwich plate under the magnetic field. An exact solution method was developed by Ebrahimi and Jafari (2017) for analyzing the vibration characteristics of magneto-electro-elastic functionally graded (MEE-FG) beams by considering porosity distribution and various boundary conditions via a four-variable shear deformation refined beam theory. Kolahchi *et al*. (2017b) studied optimization for dynamic buckling in sandwich piezoelectric nanocomposite plates based on Grey Wolf algorithm. Duc *et al*. (2017a, b, c) studied thermal and mechanical stability of a functionally graded composite truncated conical shell, plates and double curved shallow shells reinforced by carbon nanotube fibers. Based on Reddy's third-order shear deformation plate theory, the nonlinear dynamic response and vibration of imperfect functionally graded carbon nanotube-reinforced composite plates was analyzed by Thanh *et al*. (2017). Duc *et al*. (2018) presented the first analytical approach to investigate the nonlinear dynamic response and vibration of imperfect rectangular nanocompsite multilayer organic solar cell subjected to mechanical loads using the classical plate theory. A nonlocal second-order shear

deformation formulation was presented by Karami *et al*. (2018) to investigate the size-dependent thermal buckling of embedded piezoelectric sandwich nanoplates with FG core. An analytical solution of the buckling governing equations of functionally graded piezoelectric (FGP) nanobeams obtained by using a developed third-order shear deformation theory was presented by Ebrahimi and Barati (2018).

In this study, a layerwise FSDT is developed to present the buckling analysis of sandwich nanocomposite smart truncated conical shell subjected to temperature and moisture changes. The structure is consisted of a multiphase nanocomposite core and two piezoelectric layers. The Kelvin-Voigt and Halpin-Tsai models are utilized for considering structural damping effects and calculating the equivalent material properties of the core, respectively. The buckling load is calculated using DQ method. The influences of some parameters such as boundary conditions, CNTs weight percent, cone semi vertex angle, geometrical parameters, moisture and temperature changes and external voltage are investigated on the buckling load of the smart structure.

2. Halpin-Tsai model

Fig. 1 presents a sandwich smart truncated conical shell with piezoelectric layers. The core is reinforced by CNTs and carbon fibers and the top piezoelectric layer is subjected to electric field. The geometrical parameters of the truncated conical shell are r_1, and r_2 the radii of the cone at its small and large ends, respectively; α cone semi-vertex angle; L is the length of the cone; t^t, t^b and t^c respectively, actuator thickness, sensor and core layers.

Based on Halpin-Tsai model, the equivalent properties of the nanoconposite core are (Hajmohammad *et al*. 2017b)

$$E_{11} = V_F E_{11}^F + V_{MNC} E^{MNC}, \tag{1}$$

$$\frac{1}{E_{22}} = \frac{1}{E_{22}^{\mathrm{F}}} + \frac{V_{MNC}}{E^{MNC}} - V_F V_{MNC} - \frac{\dfrac{\nu_F E^{MNC}}{E_{22}^{\mathrm{F}}} + \dfrac{\nu_{MNC}^2 E_{22}^F}{E^{MNC}} - 2\nu_F \nu_{MNC}}{V_F E_{22}^{\mathrm{F}} + V_{MNC} E^{MNC}}, \tag{2}$$

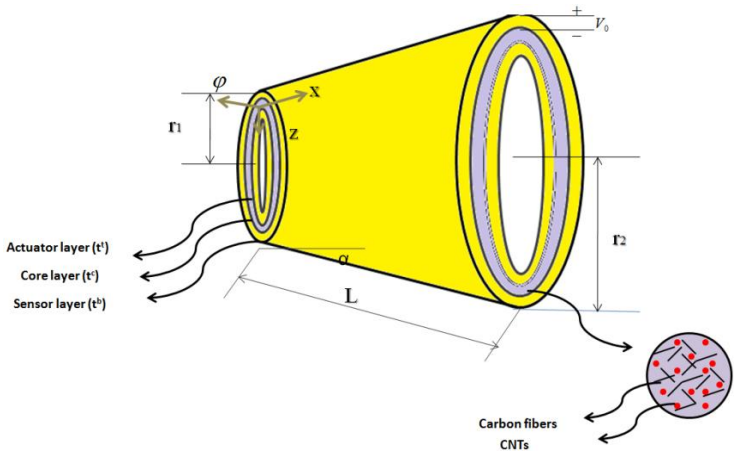

Fig. 1 A schematic of smart sandwich truncated conical shell with piezoelectric layers

$$\frac{1}{G_{12}}=\frac{V_F}{G_{12}^F}+\frac{V_{MNC}}{G^{MNC}}, \tag{3}$$

$$\rho=V_F\rho^F+V_{MNC}\rho^{MNC}, \tag{4}$$

$$\nu_{12}=V_F\nu^F+V_{MNC}\nu^{MNC}, \tag{5}$$

where G, E, V, ρ and ν are respectively, shear modulus, Young's modulus, volume fractions, density and Poisson's ratio. The subscript *MNC* and *F* show the matrix of nanocomposite and fibers, respectively. However, the elastic modulus of nanocomposite is

$$E^{MNC}=\frac{E^M}{8}\left[5\left(\frac{1+2\beta_{dd}V_{CN}}{1-\beta_{dd}V_{CN}}\right)+3\left(\frac{1+2(\ell^{CN}/\mathrm{d}^{CN})\beta_{dl}V_{CN}}{1-\beta_{dl}V_{CN}}\right)\right], \tag{6}$$

where

$$\beta_{dl}=\left(\frac{(E_{11}^{CN}/E^M)-(\mathrm{d}^{CN}/4t^{CN})}{(E_{11}^{CN}/E^M)+(\ell^{CN}/2t^{CN})}\right), \tag{7}$$

$$\beta_{dd}=\left(\frac{(E_{11}^{CN}/E^M)-(\mathrm{d}^{CN}/4t^{CN})}{(E_{11}^{CN}/E^M)+(d^{CN}/2t^{CN})}\right), \tag{8}$$

where V_M and E^M are matrix volume fraction and Young's modulus, respectively; t^{CN}, E^{CN}, ℓ^{CN}, d^{CN} and V_{CN} represent respectively, the thickness, Young's modulus, length, outer diameter and CNTs volume percent which are

$$V_{CN}=\frac{w_{CN}}{w_{CN}+\left(\rho^{CN}/\rho^m\right)-\left(\rho^{CN}/\rho^m\right)w_{CN}}, \tag{9}$$

where w_{CN}, ρ^{CN} and ρ^m are CNTs mass fraction, density of CNTs and matrix, respectively. The mass density and Poisson's ratio of the *MNC* are

$$\nu^{MNC}=\nu^M, \tag{10}$$

$$\rho^{MNC}=V_{CN}\rho^{CN}+V_M\rho^M, \tag{11}$$

$$G^{MNC}=\frac{E^{MNC}}{2(1+\nu^{MNC})}, \tag{12}$$

where ν^{MNC} and ν^M are Poisson's ratio of the *MNC* and matrix, respectively. Since the amounts of CNTs are low, the Poisson's ratio of the *MNC* and matrix are assumed equal (Hull and Clyne 2001). The transverse and longitudinal thermal expansion coefficients are

$$\alpha_x = \frac{V_F E_{11}^F \alpha_{11}^F + V_{MNC} E^{MNC} \alpha^{MNC}}{V_F E_{11}^F + V_{MNC} E^{MNC}}, \tag{13}$$

$$\alpha_\theta = (1+\nu_{12}^F) V_F \alpha_{22}^F + (1+\nu^{MNC}) V_{MNC} \alpha^{MNC} - \nu_{12} \alpha_x, \tag{14}$$

where α_{11}^F and α_{22}^F are the fiber thermal expansions and α^{MNC} is the thermal expansion of *MNC* which can be given as

$$\alpha^{MNC} = \frac{1}{2} \begin{Bmatrix} \left(\frac{V_{CN} E^{CN} \alpha^{CN} + V_M E^M \alpha^M}{V_{CN} E^{CN} + V_M E^M} \right) (1-\nu^{MNC}) \\ +(1+\nu^M) \alpha^M V_M + (1+\nu^M) \alpha^{CN} V_{CN} \end{Bmatrix}, \tag{15}$$

where α^M and α^{CN} are thermal expansion of matrix and CNTs, respectively. Here, the influence of moisture on the fiber or CNTs is neglected. The coefficients of moisture for the nanocomposite are

$$\beta_x = \frac{V_F E_{11}^F + V_{MNC} E^{MNC} \beta^M}{V_F E_{11}^F + V_{MNC} E^{MNC}}, \tag{16}$$

$$\beta_\theta = (1+\nu^{MNC}) V_{MNC} \beta^M - \nu_{12} \beta_x, \tag{17}$$

where β^M is the coefficient of moisture in the matrix. The moisture and temperature changes are assumed as

$$T = T_0 + \Delta T, \tag{18}$$

$$H = H_0 + \Delta H, \tag{19}$$

where H_0 and T_0 illustrate the moisture and temperature, respectively.

3. Layerwise FSDT

There are many new theories for modeling of different structures. Some of the new theories have been used by Tounsi and co-authors (Meziane 2014, Zidi *et al*. 2014, Attia *et al*. 2015, Zemri *et al*. 2015, Larbi Chaht *et al*. 2015, Mahi *et al*. 2015, Ahouel *et al*. 2016, El-Haina *et al*. 2017, Menasria *et al*. 2017, Chikh *et al*. 2017, Mouffoki *et al*. 2017, Khetir *et al*. 2017).

Using the layerwise FSDT, the displacements of the structure can be expressed as (Reddy 2003)

$$u^i(x,\varphi,z,t) = u_0^i(x,\varphi,t) + z^i \theta_x^i(x,\varphi,t), \tag{20}$$

$$v^i(x,\varphi,z,t) = v_0^i(x,\varphi,t) + z^i \theta_\varphi^i(x,\varphi,t), \tag{21}$$

$$w^i(x,\varphi,z,t)=w^i(x,\varphi,t), \tag{22}$$

where $i = a, s$ show the actuator and sensor layers, respectively; u_0^i, v_0^i and w^i are the mid surface displacements in the x, φ and z directions, respectively; θ_x^i and θ_φ^i are respectively rotations around x and φ curvilinear coordinates and

$$z^t = z - \left(\frac{t^t + t^c}{2}\right),\ z^b = z + \left(\frac{t^b + t^c}{2}\right). \tag{23}$$

Using Eqs. (20)-(22), the strains can be written as

$$\varepsilon_{xx}^i = \varepsilon_{0x}^i + z^i \kappa_x^i, \tag{24}$$

$$\varepsilon_{\varphi\varphi}^i = \left(\varepsilon_{0\varphi}^i + z^i \kappa_\varphi^i\right), \tag{25}$$

$$\varepsilon_{x\varphi}^i = \varepsilon_{0x\varphi}^i + \varepsilon_{0\varphi x}^i + z^i \left(\chi_{x\varphi}^i + \chi_{\varphi x}^i\right), \tag{26}$$

$$\gamma_{\varphi z}^i = \gamma_{o\varphi z}^i, \tag{27}$$

$$\gamma_{xz}^i = \gamma_{oxz}^i, \tag{28}$$

where

$$\varepsilon_{0x}^i = \frac{\partial u_0^i}{\partial x}, \kappa_x^i = \frac{\partial \theta_x^i}{\partial x} \tag{29}$$

$$\varepsilon_{0\varphi}^i = \frac{1}{x\sin\alpha}\frac{\partial v_0^i}{\partial \varphi} + \frac{u_0^i}{x} + \frac{w_0^i}{x\tan\varphi}, \qquad \kappa_\varphi^i = \frac{1}{x\sin\alpha}\frac{\partial \theta_\varphi^i}{\partial \varphi} + \frac{\theta_x^i}{x} \tag{30}$$

$$\varepsilon_{0x\varphi}^i = \frac{\partial v_0^i}{\partial x}, \qquad \varepsilon_{0\varphi x}^i = \frac{1}{x\sin\alpha}\frac{\partial u_0^i}{\partial \varphi} - \frac{v_0^i}{x}, \quad \chi_{x\varphi}^i = \frac{\partial \theta_\varphi^i}{\partial x}, \quad \chi_{\varphi x}^i = \frac{1}{x\sin\alpha}\frac{\partial \theta_x^i}{\partial \varphi} - \frac{\theta_\varphi^i}{x} \tag{31}$$

$$\gamma_{0\varphi z}^i = \frac{1}{x\sin\alpha}\frac{\partial w_0^i}{\partial \varphi} - \frac{v_0^i}{x\tan\varphi} + \theta_\varphi^i, \tag{32}$$

$$\gamma_{0xz}^i = \frac{\partial w_0^i}{\partial x} + \theta_x^i, \tag{33}$$

The boundary conditions of continuity between layers are

$$\begin{cases} u^c\big|_{z=\frac{t^c}{2}} = u^t\big|_{z=\frac{t^c}{2}} \\ u^c\big|_{z=-\frac{t^c}{2}} = u^b\big|_{z=-\frac{t^c}{2}} \end{cases}, \begin{cases} v^c\big|_{z=\frac{t^c}{2}} = v^t\big|_{z=\frac{t^c}{2}} \\ v^c\big|_{z=-\frac{t^c}{2}} = v^b\big|_{z=-\frac{t^c}{2}} \end{cases}, \begin{cases} w^c\big|_{z=\frac{t^c}{2}} = w^t\big|_{z=\frac{t^c}{2}} \\ w^c\big|_{z=-\frac{t^c}{2}} = w^b\big|_{z=-\frac{t^c}{2}} \end{cases} \tag{34}$$

Substituting Eq. (34) into Eqs. (20)-(22) yields

$$u_0^c = \frac{u_0^t + u_0^b}{2} + \frac{1}{4}\left(t^b \theta_x^b - t^t \theta_x^t\right), \tag{35}$$

$$\theta_x^c = \frac{u_0^t - u_0^b}{t^c} - \frac{1}{2t^c}\left(t^b \theta_x^b + t^t \theta_x^t\right), \tag{36}$$

$$v_0^c = \frac{v_0^t + v_0^b}{2} + \frac{1}{4}\left(t^b \theta_\varphi^b - t^t \theta_\varphi^t\right), \tag{37}$$

$$\theta_\varphi^c = \frac{v_0^t - v_0^b}{t^c} - \frac{1}{2t^c}\left(t^b \theta_\varphi^b + t^t \theta_\varphi^t\right), \tag{38}$$

$$w_0^c = \frac{w^t + w^b}{2}, \tag{39}$$

4. Piezoelasticity theory

The basic equation of the piezoelasticity theory is (Kolahchi *et al*. 2016a)

$$\begin{bmatrix} \sigma_{xx}^i \\ \sigma_{\varphi\varphi}^i \\ \sigma_{\varphi z}^i \\ \sigma_{xz}^i \\ \sigma_{x\varphi}^i \\ D_x^k \\ D_\varphi^k \\ D_z^k \end{bmatrix} = \begin{bmatrix} Q_{11}^i & Q_{12}^i & 0 & 0 & 0 & 0 & 0 & -e_{31}^k \\ Q_{21}^i & Q_{22}^i & 0 & 0 & 0 & 0 & 0 & -e_{32}^k \\ 0 & 0 & Q_{44}^i & 0 & 0 & 0 & -e_{24}^k & 0 \\ 0 & 0 & 0 & Q_{55}^i & 0 & -e_{15}^k & 0 & 0 \\ 0 & 0 & 0 & 0 & Q_{66}^i & 0 & 0 & 0 \\ 0 & 0 & 0 & -e_{15}^k & 0 & \in_{11}^k & 0 & 0 \\ 0 & 0 & -e_{23}^k & 0 & 0 & 0 & \in_{22}^k & 0 \\ -e_{31}^k & -e_{32}^k & 0 & 0 & 0 & 0 & 0 & \in_{33}^k \end{bmatrix} \begin{bmatrix} \varepsilon_{xx}^i - \alpha_{xx}^i \Delta T^i - \beta_{xx}^i \Delta H^i \\ \varepsilon_{\varphi\varphi}^i - \alpha_{\varphi\varphi}^i \Delta T^i - \beta_{\varphi\varphi}^i \Delta H^i \\ \gamma_{\varphi z}^i \\ \gamma_{xz}^i \\ \gamma_{x\varphi}^i \\ E_x^k \\ E_\varphi^k \\ E_z^k \end{bmatrix}, \tag{40}$$

where the terms Q_{jm}^i, e_{ij}^k and $\in_{ii}^k$ are elastic, piezoelectric and dielectric constants, respectively; β_{xx}, $\beta_{\varphi\varphi}$ and α_{xx}, $\alpha_{\varphi\varphi}$ are respectively moisture coefficients and thermal expansion; ΔH and ΔT are moisture and temperature different, respectively; D_m^k and E_m^k are the electric displacement and electric field, respectively which the last can be expressed as a function of electric potential (i.e., ϕ^i) as

$$E_m^k = -\frac{\partial \phi^k}{\partial m}, \; m = x, \mathrm{r}\varphi, z \tag{41}$$

The distribution of electric potential across the thickness of the actuator is

$$\phi^a(x, \varphi, z, t) = \sin\left(\frac{\pi(z - t^c/2)}{t^t}\right)\Phi^a(x, \varphi, t) + \frac{(z - t^c/2)V_0}{t^t}, \tag{42}$$

$$\phi^s(x,\varphi,z,t)=\sin\left(\frac{\pi(-z-t^c/2)}{t^b}\right)\Phi^s(x,\varphi,t), \tag{43}$$

where $\Phi^k(x, \varphi, t)$ is the electric potential and V_0 is the external voltage. Noted that super index k is related to actuator (a) and sensor (s) layers.

Neglecting the dielectric and piezoelectric constants in Eq. (40), the stresses of the multiphase nanocomposite core can be derived.

5. Governing equations

The energy of potential for the system is

$$\begin{aligned}U=&\frac{1}{2}\int_A\int\left(\sigma^i_{jm}\varepsilon^i_{jm}\right)dzdA-\frac{1}{2}\left(\int_A\int_{t^c/2}^{\left(t^c/2+t^t\right)}\left[D^a_x\left(-\sin\left(\frac{\pi(z-t^c/2)}{t^t}\right)\frac{\partial\Phi^a}{\partial x}\right)\right.\right.\\&+D^a_\varphi\left(-\sin\left(\frac{\pi(z-t^c/2)}{t^t}\right)\frac{\partial\Phi^a}{r\partial\varphi}\right)+D^a_z\left(-\frac{\pi}{2}\cos\left(\frac{\pi(z-t^c/2)}{t^t}\right)\Phi^{(a)}-\frac{V_0}{2}\right)\left.\right]dzdA\\&+\left(\int_A\int_{-\left(t^c/2+t^b\right)}^{-t^c/2}\left[D^s_x\left(-\sin\left(\frac{\pi(-z-t^c/2)}{t^b}\right)\frac{\partial\Phi^s}{\partial x}\right)\right.\right.\\&+D^s_\varphi\left(-\sin\left(\frac{\pi(-z-t^c/2)}{t^b}\right)\frac{\partial\Phi^s}{r\partial\varphi}\right)+D^s_z\left(\frac{\pi}{2}\cos\left(\frac{\pi(-z-t^c/2)}{t^b}\right)\Phi^s\right)\left.\right]dzdA\left.\right),\end{aligned} \tag{44}$$

The internal force due to the moisture and thermal loads as well as mechanical load can be written as

$$W=-\frac{1}{2}\left[\int N^m_x\left(\frac{\partial w^t}{\partial x}\right)^2dx+\int N^m_x\left(\frac{\partial w^c}{\partial x}\right)^2dx+\int N^m_x\left(\frac{\partial w^b}{\partial x}\right)^2dx\right] \tag{45}$$

where

$$N^m_x=N^E_x-\sum^{i=a,c,s}\int\left(Q^i_{11}\alpha^i_{xx}+Q^i_{12}\alpha^i_{\varphi\varphi}\right)\Delta T^i dz-\sum^{i=a,c,s}\int\left(Q^i_{11}\beta^i_{xx}+Q^i_{12}\beta^i_{\varphi\varphi}\right)\Delta H^i dz, \tag{46}$$

where N^E_x is the external mechanical load applied to the structure in x-direction. Applying Hamilton's principle, the equations of motion for $\delta u^t_0, \delta v^t_0, \delta w^t, \delta\theta^t_x, \delta\theta^t_\varphi, \delta u^c_2, \delta v^c_2, \delta w^c_2, \delta u^c_3, \delta v^c_3, \delta w^c_3, \delta u^b_0, \delta v^b_0, \delta w^b, \delta\theta^b_x, \delta\theta^b_\varphi$ can be derived as

$$\begin{aligned}&\left(\frac{1}{2x}\right)\left\{N^c_x\right\}+\left(\frac{1}{2}\right)\left\{N^c_{x,x}\right\}+\left(\frac{1}{t^cx}\right)\left\{M^c_x\right\}+\left(\frac{1}{t^c}\right)\left\{M^c_{x,x}\right\}-\left(\frac{1}{2x}\right)\left\{N^c_\varphi\right\}-\left(\frac{1}{t^cx}\right)\left\{M^c_\varphi\right\}+\\&\left(\frac{1}{2x\sin\alpha}\right)\left\{N^c_{\varphi x,\varphi}\right\}+\left(\frac{1}{t^cx\sin\alpha}\right)\left\{M^c_{\varphi x,\varphi}\right\}-\left(\frac{1}{t^c}\right)\left\{Q^c_{zx}\right\}+\left(\frac{1}{x}\right)\left\{N^t_x\right\}+\left\{N^t_{x,x}\right\}-\left(\frac{1}{x}\right)\left\{N^t_\varphi\right\}+\\&\left(\frac{1}{x\sin\alpha}\right)\left\{N^t_{\varphi x,\varphi}\right\}=0,\end{aligned} \tag{47a}$$

$$\left(\frac{h_\varphi}{2x\sin\alpha}\right)\{N^{\,c}_{\varphi,\varphi}\}+\left(\frac{h_\varphi}{t^c x\sin\alpha}\right)\{M^{\,c}_{\varphi,\varphi}\}+\left(\frac{h_{x\varphi}}{2x}\right)\{N^{\,c}_{x\varphi}\}+\left(\frac{h_{x\varphi}}{2}\right)\{N^{\,c}_{x\varphi,x}\}+\left(\frac{h_{x\varphi}}{2x}\right)\{N^{\,c}_{\varphi x}\}+$$
$$\left(\frac{h_{x\varphi}}{t^c x}\right)\{M^{\,c}_{x\varphi}\}+\left(\frac{h_{x\varphi}}{t^c}\right)\{M^{\,c}_{x\varphi,x}\}+\left(\frac{h_{x\varphi}}{t^c x}\right)\{M^{\,c}_{\varphi x}\}+\left(\frac{1}{2x\tan\alpha}\right)\{Q^{c}_{\varphi z}\}+\left(\frac{1}{t^c x\tan\alpha}\right)\{S^{\,c}_{\varphi z}\}- \tag{47b}$$
$$\left(\frac{1}{t^c}\right)\{Q^{c}_{z\varphi}\}+\left(\frac{1}{x\sin\alpha}\right)\{N^{\,t}_{\varphi,\varphi}\}+\left(\frac{1}{x}\right)\{N^{\,t}_{x\varphi}\}+\{N^{\,t}_{x\varphi,x}\}+\left(\frac{1}{x}\right)\{N^{\,t}_{\varphi x}\}+\left(\frac{k_s}{x\tan\alpha}\right)\{Q^{t}_{\varphi z}\}=0,$$

$$-\left(\frac{h_\varphi}{2x\tan\varphi}\right)\{N^{\,c}_{\varphi}\}-\left(\frac{h_\varphi}{t^c x\tan\varphi}\right)\{M^{\,c}_{\varphi}\}+\left(\frac{1}{2x}\right)\{Q^{c}_{xz}\}+\left(\frac{1}{2}\right)\{Q^{c}_{xz,x}\}+$$
$$\left(\frac{1}{xt^c}\right)\{S^{\,c}_{xz}\}+\left(\frac{1}{t^c}\right)\{S^{\,c}_{xz,x}\}+\left(\frac{1}{2x\sin\varphi}\right)\{Q^{c}_{\varphi z,\varphi}\}+\left(\frac{1}{x\sin\varphi t^c}\right)\{S^{\,c}_{\varphi z,\varphi}\}- \tag{47c}$$
$$\left(\frac{1}{x\sin\varphi}\right)\{N^{\,t}_{\varphi}\}+\left(\frac{k_s}{x}\right)\{Q^{t}_{xz}\}+k_s\{Q^{t}_{xz,x}\}+\left(\frac{k_s}{x\sin\varphi}\right)\{Q^{t}_{\varphi z,\varphi}\}+$$
$$N^{\,m}_{x}\left(w^{\,t}_{,xx}+\frac{1}{4}\left(w^{\,t}_{,xx}+w^{\,b}_{,xx}\right)\right)=0,$$

$$-\left(\frac{h_x t^t}{4x}\right)\{N^{\,c}_{x}\}-\left(\frac{h_x t^t}{4}\right)\{N^{\,c}_{x,x}\}-\left(\frac{h_x t^t}{2xt^c}\right)\{M^{\,c}_{x}\}-\left(\frac{h_x t^t}{2t^c}\right)\{M^{\,c}_{x,x}\}+\left(\frac{h_\varphi t^t}{4x}\right)\{N^{\,c}_{\varphi}\}+\left(\frac{h_\varphi t^t}{2xt^c}\right)\{M^{\,c}_{\varphi}\}-$$
$$\left(\frac{h_{x\varphi}t^t}{4x\sin\alpha}\right)\{N^{\,c}_{\varphi x,\varphi}\}-\left(\frac{h_{x\varphi}t^t}{2x\sin\alpha t^c}\right)\{M^{\,c}_{\varphi x,\varphi}\}+\left(\frac{t^t}{2t^c}\right)\{Q^{c}_{zx}\}+\left(\frac{1}{x}\right)\{M^{\,t}_{x}\}+\{M^{\,t}_{x,x}\}-\left(\frac{1}{x}\right)\{M^{\,t}_{\varphi}\}+ \tag{47d}$$
$$\left(\frac{1}{x\sin\alpha}\right)\{M^{\,t}_{\varphi x,\varphi}\}-k_s\{Q^{t}_{zx}\}=0,$$

$$-\left(\frac{h_\varphi t^t}{4x\,sin\,\varphi}\right)\{N^{c}_{\varphi,\varphi}\}-\left(\frac{h_\varphi t^t}{2x\,sin\,\varphi\,t^c}\right)\{M^{c}_{\varphi,\varphi}\}-\left(\frac{h_{x\varphi}t^t}{4x}\right)\{N^{c}_{\varphi x}\}-\left(\frac{h_{x\varphi}t^t}{4x}\right)\{N^{c}_{x\varphi}\}$$
$$-\left(\frac{h_{x\varphi}t^t}{4}\right)\{N^{c}_{x\varphi,x}\}-\left(\frac{h_{x\varphi}t^t}{2xt^c}\right)\{M^{c}_{\varphi x}\}-\left(\frac{h_{x\varphi}t^t}{2xt^c}\right)\{M^{c}_{x\varphi}\}-\left(\frac{h_{x\varphi}t^t}{2t^c}\right)\{M^{c}_{x\varphi,x}\}$$
$$-\left(\frac{t^t}{4x\,tan\,\varphi}\right)\{Q^{c}_{\varphi z}\}-\left(\frac{t^t}{2t^c x\,tan\,\varphi}\right)\{S^{c}_{\varphi z}\}+\left(\frac{t^t}{2t^c}\right)\{Q^{c}_{z\varphi}\}+\left(\frac{1}{x\,sin\,\varphi}\right)\{M^{t}_{\varphi,\varphi}\}$$
$$+\left(\frac{1}{x}\right)\{M^{t}_{\varphi x}\}+\left(\frac{1}{x}\right)\{M^{t}_{x\varphi}\}+\{M^{t}_{x\varphi,x}\}+\left(\frac{k_s}{x\,tan\,\varphi}\right)\{S^{t}_{\varphi z}\}-k_s\{Q^{t}_{z\varphi}\} \tag{47e}$$
$$=\left[\left(-\frac{t^t}{8}I^c_0-\frac{t^t}{2t^c}I^c_1-\frac{t^t}{2t^{c\,2}}I^c_2\right)+I^t_1\right]\ddot{v}^t_0+\left[\left(\frac{t^{t\,2}}{16}I^c_0+\frac{t^{t\,2}}{4t^c}I^c_1+\frac{t^{t\,2}I^c_2}{4t^{c\,2}}\right)+I^t_2\right]\ddot{\theta}^t_\varphi$$
$$+\left[\frac{t^t t^{c\,2}}{16}I^c_0+\frac{t^t t^c}{8}I^c_1-\frac{t^t}{4}I^c_2-\frac{t^t}{2t^c}I^c_3\right]\ddot{v}^c_2+\left[\frac{t^t t^{c\,2}}{16}I^c_1+\frac{t^t t^c}{8}I^c_2-\frac{t^t}{4}I^c_3-\frac{t^t}{2t^c}I^c_4\right]\ddot{v}^c_3$$
$$+\left[-\frac{t^t}{8}I^c_0+\frac{t^t}{2t^{c\,2}}I^c_2\right]\ddot{v}^b_0+\left[-\frac{t^t t^b}{16}I^c_0+\frac{t^t t^b}{4t^{c\,2}}I^c_2\right]\ddot{\theta}^b_\varphi$$

$$\left(\frac{h_x}{2x}\right)\{N^{c}_{x}\}+\left(\frac{h_x}{2}\right)\{N^{c}_{x,x}\}-\left(\frac{h_x}{xt^{c}}\right)\{M^{c}_{x}\}-\left(\frac{h_x}{t^{c}}\right)\{M^{c}_{x,x}\}-\left(\frac{h_\varphi}{2x}\right)\{N^{c}_{\varphi}\}+\left(\frac{h_\varphi}{xt^{c}}\right)\{M^{c}_{\varphi}\}+$$
$$\left(\frac{h_{x\varphi}}{2x\sin\varphi}\right)\{N^{c}_{\varphi x,\varphi}\}-\left(\frac{h_{x\varphi}}{x\sin\varphi t^{c}}\right)\{M^{c}_{\varphi x,\varphi}\}+\left(\frac{1}{t^{c}}\right)\{Q^{c}_{zx}\}+\left(\frac{1}{x}\right)\{N^{b}_{x}\}+\{N^{b}_{x,x}\}-\left(\frac{1}{x}\right)\{N^{b}_{\varphi}\}+ \quad (47f)$$
$$\left(\frac{1}{x\sin\varphi}\right)\{N^{b}_{\varphi x,\varphi}\}=0,$$

$$\left(\frac{h_\varphi}{2x\sin\alpha}\right)\{N^{c}_{\varphi,\varphi}\}-\left(\frac{h_\varphi}{t^{c}x\sin\alpha}\right)\{M^{c}_{\varphi,\varphi}\}+\left(\frac{h_{x\varphi}}{2x}\right)\{N^{c}_{x\varphi}\}+\left(\frac{h_{x\varphi}}{2}\right)\{N^{c}_{x\varphi,x}\}+\left(\frac{h_{x\varphi}}{2x}\right)\{N^{c}_{\varphi x}\}-$$
$$\left(\frac{h_{x\varphi}}{xt^{c}}\right)\{M^{c}_{x\varphi}\}-\left(\frac{h_{x\varphi}}{t^{c}}\right)\{M^{c}_{x\varphi,x}\}-\left(\frac{h_{x\varphi}}{xt^{c}}\right)\{M^{c}_{\varphi x}\}+\left(\frac{1}{2x\tan\alpha}\right)\{Q^{c}_{\varphi z}\}-\left(\frac{1}{t^{c}x\tan\alpha}\right)\{S^{c}_{\varphi z}\}+ \quad (47g)$$
$$\left(\frac{1}{t^{c}}\right)\{Q^{c}_{z\varphi}\}+\left(\frac{1}{x\sin\alpha}\right)\{N^{b}_{\varphi,\varphi}\}+\left(\frac{1}{x}\right)\{N^{b}_{x\varphi}\}+\{N^{b}_{x\varphi,x}\}+\left(\frac{1}{x}\right)\{N^{b}_{\varphi x}\}+\left(\frac{k_s}{x\tan\alpha}\right)\{Q^{b}_{\varphi z}\}=0,$$

$$-\left(\frac{h_\varphi}{2x\tan\alpha}\right)\{N^{c}_{\varphi}\}+\left(\frac{h_\varphi}{t^{c}x\tan\alpha}\right)\{M^{c}_{\varphi}\}+\left(\frac{1}{2x}\right)\{Q^{c}_{xz}\}+\left(\frac{1}{2}\right)\{Q^{c}_{xz,x}\}-\left(\frac{1}{xt^{c}}\right)\{S^{c}_{xz}\}-\left(\frac{1}{t^{c}}\right)\{S^{c}_{xz,x}\}+$$
$$\left(\frac{1}{2x\sin\alpha}\right)\{Q^{c}_{\varphi z,\varphi}\}-\left(\frac{1}{x\sin\alpha t^{c}}\right)\{S^{c}_{\varphi z,\varphi}\}-\left(\frac{1}{x\sin\alpha}\right)\{N^{b}_{\varphi}\}+\left(\frac{k_s}{x}\right)\{Q^{b}_{xz}\}+k_s\{Q^{b}_{xz,x}\}+\left(\frac{k_s}{x\tan\alpha}\right)\{Q^{b}_{\varphi z,\varphi}\} \quad (47h)$$
$$+N^{m}_{x}\left(w^{b}_{,xx}+\frac{1}{4}\left(w^{t}_{,xx}+w^{b}_{,xx}\right)\right)=0,$$

$$\left(\frac{h_x t^{b}}{4x}\right)\{N^{c}_{x}\}+\left(\frac{h_x t^{b}}{4}\right)\{N^{c}_{x,x}\}-\left(\frac{h_x t^{b}}{2xt^{c}}\right)\{M^{c}_{x}\}-\left(\frac{h_x t^{b}}{2t^{c}}\right)\{M^{c}_{x,x}\}-\left(\frac{h_\varphi t^{b}}{4x}\right)\{N^{c}_{\varphi}\}+\left(\frac{h_\varphi t^{b}}{2xt^{c}}\right)\{M^{c}_{\varphi}\}$$
$$+\left(\frac{h_{x\varphi}t^{b}}{4x\sin\alpha}\right)\{N^{c}_{\varphi x,\varphi}\}-\left(\frac{h_{x\varphi}t^{b}}{2x\sin\alpha t^{c}}\right)\{M^{c}_{\varphi x,\varphi}\}+\left(\frac{t^{b}}{2t^{c}}\right)\{Q^{c}_{zx}\}+\left(\frac{1}{x}\right)\{M^{b}_{x}\}+\{M^{b}_{x,x}\}-\left(\frac{1}{x}\right)\{M^{b}_{\varphi}\}+ \quad (47i)$$
$$\left(\frac{1}{x\sin\alpha}\right)\{M^{b}_{\varphi x,\varphi}\}-k_s\{Q^{b}_{zx}\}=0,$$

$$\left(\frac{h_\varphi t^{b}}{4x\sin\alpha}\right)\{N^{c}_{\varphi,\varphi}\}-\left(\frac{h_\varphi t^{b}}{2x\sin\alpha t^{c}}\right)\{M^{c}_{\varphi,\varphi}\}+\left(\frac{h_{x\varphi}t^{b}}{4x}\right)\{N^{c}_{\varphi x}\}+\left(\frac{h_{x\varphi}t^{b}}{4x}\right)\{N^{c}_{x\varphi}\}+\left(\frac{h_{x\varphi}t^{b}}{4}\right)\{N^{c}_{x\varphi,x}\}-$$
$$\left(\frac{h_{x\varphi}t^{b}}{2xt^{c}}\right)\{M^{c}_{\varphi x}\}-\left(\frac{h_{x\varphi}t^{b}}{2xt^{c}}\right)\{M^{c}_{x\varphi}\}-\left(\frac{h_{x\varphi}t^{b}}{2t^{c}}\right)\{M^{c}_{x\varphi,x}\}+\left(\frac{t^{b}}{4x\tan\alpha}\right)\{Q^{c}_{\varphi z}\}-\left(\frac{t^{b}}{2t^{c}x\tan\alpha}\right)\{S^{c}_{\varphi z}\}+ \quad (47j)$$
$$\left(\frac{t^{b}}{2t^{c}}\right)\{Q^{c}_{z\varphi}\}+\left(\frac{1}{x\sin\alpha}\right)\{M^{b}_{\varphi,\varphi}\}+\left(\frac{1}{x}\right)\{M^{b}_{\varphi x}\}+\left(\frac{1}{x}\right)\{M^{b}_{x\varphi}\}+\{M^{b}_{x\varphi,x}\}+\left(\frac{k_s}{x\tan\alpha}\right)\{S^{b}_{\varphi z}\}-k_s\{Q^{b}_{z\varphi}\}=0,$$

$$\delta\Phi^a:\int_{tc/2}^{(tc/2+ta)}\left[\left(\sin\left(\frac{\pi(z-tc/2)}{ta}\right)\frac{\partial D_x^a}{\partial x}\right)+\left(\sin\left(\frac{\pi(z-tc/2)}{ta}\right)\frac{\partial D_\varphi^a}{r\partial\varphi}\right)-\left(\frac{\pi}{2}\cos\left(\frac{\pi(z-tc/2)}{ta}\right)D_z^a\right)\right]dz\,, \tag{47k}$$

$$\delta\Phi^s:\int_{-(tc/2+ts)}^{-tc/2}\left[\left(\sin\left(\frac{\pi(-z-tc/2)}{ts}\right)\frac{\partial D_x^s}{\partial x}\right)+\left(\sin\left(\frac{\pi(-z-tc/2)}{ts}\right)\frac{\partial D_\varphi^s}{r\partial\varphi}\right)+\left(\frac{\pi}{2}\cos\left(\frac{\pi(-z-tc/2)}{ts}\right)D_z^s\right)\right]dz\,. \tag{47l}$$

where the force resultants are

$$\begin{bmatrix} N_\alpha^i & M_\alpha^i \\ N_\beta^i & M_\beta^i \\ N_{\alpha\beta}^i & M_{\alpha\beta}^i \\ N_{\beta\alpha}^i & M_{\beta\alpha}^i \end{bmatrix}=\int_{z^i}\begin{Bmatrix}\sigma_{xx}\\ \sigma_{\varphi\varphi}\\ \tau_{x\varphi}\\ \tau_{\varphi x}\end{Bmatrix}^i\left(1,z^i\right)dz^i\,, \tag{48}$$

$$\begin{bmatrix} Q_{\beta z}^i & S_{\beta z}^i \\ Q_{z\beta}^i & 0 \\ Q_{\alpha z}^i & S_{\alpha z}^i \\ Q_{z\alpha}^i & 0 \end{bmatrix}=\int_{z^i}\begin{Bmatrix}\tau_{\varphi z}\\ \tau_{z\varphi}\\ \tau_{xz}\\ \tau_{zx}\end{Bmatrix}^i\left(1,z^i\right)dz^i\,, \tag{49}$$

The assumed boundary conditions (BCs) are

- **Simply-Simply (SS)**

$$v^i=w^i=\theta_x^i=N_x^i=M_x^i=0,\qquad \text{on both ends} \tag{50}$$

- **Clamped-Clamped (CC)**

$$u^i=v^i=w^i=\theta_x^i=\theta_\varphi^i=0,\qquad \text{on both ends} \tag{51}$$

- **Clamped-Simply (CS)**

$$\begin{aligned} u^i=v^i=w^i=\theta_x^i=\theta_\varphi^i=0 \quad at \quad x=0\\ v^i=w^i=\theta_x^i=N_x^i=M_x^i=0 \quad at \quad x=L\end{aligned} \tag{52}$$

6. DQM

Using DQM, the differential equations are changed to algebraic one based on the following equations (Kolahchi *et al*. 2016b, Kolahchi 2017c, Zarei *et al*. 2017)

$$\frac{d^n F(x_i,\varphi_j)}{dx^n}=\sum_{k=1}^{N_x} A_{ik}^{(n)} F(x_k,\varphi_j) \qquad n=1,...,N_x-1, \tag{53}$$

$$\frac{d^m F(x_i,\varphi_j)}{d\varphi^m}=\sum_{l=1}^{N_\varphi} B_{jl}^{(m)} F(x_i,\varphi_l) \qquad m=1,...,N_\varphi-1, \tag{54}$$

$$\frac{d^{n+m} F(x_i,\varphi_j)}{dx^n d\varphi^m}=\sum_{k=1}^{N_x}\sum_{l=1}^{N_\varphi} A_{ik}^{(n)} B_{jl}^{(m)} F(x_k,\varphi_l), \tag{55}$$

where $A_{ik}^{(n)}$ and $B_{jl}^{(m)}$ are the weighting coefficients which may be expressed as

$$A_{ij}^{(1)}=\begin{cases} \dfrac{\prod_{\substack{j=1\\ j\neq i}}^{N_x}(x_i-x_j)}{(x_i-x_j)\prod_{\substack{j=1\\ j\neq i}}^{N_x}(x_i-x_j)} & for \quad i\neq j, \quad i,j=1,2,...,N_x \\ -\sum_{\substack{j=1\\ i\neq j}}^{N_x} A_{ij}^{(1)} & for \quad i=j, \quad i,j=1,2,...,N_x \end{cases} \tag{56}$$

$$B_{ij}^{(1)}=\begin{cases} \dfrac{\prod_{\substack{j=1\\ j\neq i}}^{N_\phi}(\phi_i-\phi_j)}{(\phi_i-\phi_j)\prod_{\substack{j=1\\ j\neq i}}^{N_\phi}(\phi_i-\phi_j)} & for \quad i\neq j, \quad i,j=1,2,...,N_\phi, \\ -\sum_{\substack{j=1\\ i\neq j}}^{N_\phi} B_{ij}^{(1)} & for \quad i=j, \quad i,j=1,2,...,N_\phi \end{cases} \tag{57}$$

The weighting coefficients for the second, third and fourth derivatives can be determined via multiplication of weighting coefficients in each others.

In addition, the grid points distribution can be calculated from

$$x_i=\frac{L}{2}\left[1-\cos\left(\frac{i-1}{N_x-1}\right)\pi\right] \qquad i=1,...,N_x \tag{58}$$

$$\varphi_i=\frac{2\pi}{2}\left[1-\cos\left(\frac{i-1}{N_\varphi-1}\right)\pi\right] \qquad i=1,...,N_\varphi \tag{59}$$

Using DQM, the motion equations can be expressed as

$$\begin{bmatrix} K_{bb} & K_{bd} \\ K_{db} & K_{dd} \end{bmatrix} \begin{bmatrix} Y_b \\ Y_d \end{bmatrix} + F \begin{bmatrix} K_{bb}^G & K_{bd}^G \\ K_{db}^G & K_{dd}^G \end{bmatrix} \begin{bmatrix} Y_b \\ Y_d \end{bmatrix} = \begin{bmatrix} 0 \\ 0 \end{bmatrix}, \tag{60}$$

where $[K]$ is the stiffness matrix; $[K^G]$ shows the matrix of force coefficients; F is the buckling load; $\{Y\}$ is the displacement vector; subscripts b and d indicate the boundary and domain points. Eliminating the boundary points in Eq. (60), we have

$$Y_b = -\left([K_{bb}]^{-1}[K_{bd}]\right)Y_d, \tag{61}$$

Substituting Eqs. (61) into Eq. (60) yields

$$[K^*]Y + F[KG^*]Y_d = 0, \tag{62}$$

where

$$[KG^*] = [K_{dd}^G] - [K_{db}^G][K_{bb}]^{-1}[K_{bd}], \tag{63}$$

$$[K^*] = [K_{dd}] - [K_{db}][K_{bb}]^{-1}[K_{bd}]. \tag{64}$$

Finally, Eq. (62) should be solved to calculate the buckling load of the structure.

7. Numerical results

A sandwich piezoelectric truncated conical shell with cone semi vertex angle of α = 30 and length to cone large radius ratio of L/r_2 = 2 is assumed. The core is from Epoxy armed by carbon fibers and CNTs with the properties shown in Table 1 (Hajmohammad *et al*. 2017b).

The smart layers are from PZT-5 with the moisture and temperature-dependent material properties as

$$E_{11} = E_{110}\left(1 + E_{111}\Delta T\right) \tag{65a}$$

$$E_{22} = E_{220}\left(1 + E_{221}\Delta T\right) \tag{65b}$$

$$G_{12} = G_{120}\left(1 + G_{121}\Delta T\right) \tag{65c}$$

$$G_{13} = G_{130}\left(1 + G_{131}\Delta T\right) \tag{65d}$$

$$G_{23} = G_{230}\left(1 + G_{231}\Delta T\right) \tag{65e}$$

$$\alpha_{xx} = \alpha_{110}\left(1 + \alpha_{111}\Delta T\right) \tag{65f}$$

$$\alpha_{\theta\theta} = \alpha_{220}\left(1 + \alpha_{221}\Delta T\right) \tag{65g}$$

$$\beta_{xx} = \beta_{110}\left(1 + \alpha_{111}\Delta H\right) \tag{65h}$$

Table 1 Material properties of Epoxy, CNTs and carbon fibers

Material	Properties
Epoxy	Young's modulus: $E^M = (3.51 - 0.0034T + 0.142H)$ GPa, Poisson's ratio: $v^M = 0.3$, Density: $\rho^M = 1200$ Kg/m^3, Thermal expansion coefficient: $\alpha^M = 45(1 + 0.0001\,\Delta T) \times 10^{-6}\,K^{-1}$, Moisture coefficient: $\beta^M = 2.68 \times 10^{-3}$ wt%$^{-1}$
Carbon fibers	Young's modulus: $E_{11}^F = 233.05\ GPa$ and $E_{22}^F = 23.1\ GPa$, Shear modulus: $G_{12}^F = 8.96\ GPa$, Poisson's ratio: $v^F = 0.2$, Density: $\rho^F = 1750$ Kg/m^3, Thermal expansion coefficient: $\alpha_{xx}^F = -0.54 \times 10^{-6}\,K^{-1}$ and $\alpha_{\varphi\varphi}^F = 10.8 \times 10^{-6}\,K^{-1}$, Volume percent: $V^F = 0.6$
CNTs	Young's modulus: $E^{CN} = 640(1 - 0.0005\Delta T)$ GPa, Poisson's ratio: $v^{CN} = 0.27$, Density: $\rho^{CN} = 1350$ Kg/m^3, Outer diameter: $d^{CN} = 1.4$ nm, Thickness: $t^{CN} = 0.34$ nm, Length: $\ell^{CN} = 25\times10^{-6}$ m, Thermal expansion coefficient: $\alpha^{CN} = 4.5361\times10^{-6}\,K^{-1}$ and $\alpha^{CN} = 4.6677\times10^{-6}\,K^{-1}$, respectively at $T = 300\,K$, $T = 500\,K$ and $T = 7700\,K$.

Table 2 Material property of PZT-5

Elastic constants	Piezoelectric constants	Thermal and moisture coefficients
$E_{110} = E_{220} = 61$ GPa $E_{330} = 53.2$ GPa $G_{120} = G_{130} = G_{230} = 24.2$ GPa $\upsilon_{12} = 0.35$ $\upsilon_{23} = \upsilon_{13} = 0.38$ $E_{111} = -0.0005$ $E_{221} = E_{331} = G_{121} = G_{131} = G_{231} = -0.0002$	$d_{31} = d_{32} = -1.71\times10^{-10}$ m/V $d_{24} = d_{15} = 5.84\times10^{-10}$ m/V $d_{33} = 3.74\times10^{-10}$ m/V	$\alpha_{120} = \alpha_{220} = 0.9\times10^{-6}$ 1/K $\alpha_{111} = \alpha_{221} = 0.0005$ $\beta_{120} = \beta_{220} = 2.68\times10^{-3}$ wt%$^{-1}$ $\beta_{111} = \beta_{221} = 0.001$

$$\beta_{\varphi\varphi} = \beta_{220}\left(1 + \alpha_{221}\Delta H\right) \tag{65i}$$

where the constants are listed in Table 2.

7.1 Accuracy and convergence of DQM

The accuracy and convergence of the DQM is studied in Fig. 2 where the non-dimensional buckling load ($P = F/(LE^M)$) is plotted versus the grid point number. It is found that the non dimensional buckling load is decreased with enhancing the numbers of grid point until in $N = 15$, the results become converge.

7.2 Validation

Since the buckling of smart sandwich truncated conical shell is studied in this paper for the first time, for validation we should neglect the effect of CNTs and carbon fibers in the core, top and bottom layers, hygrothermal load and structural damping. However, buckling analysis of

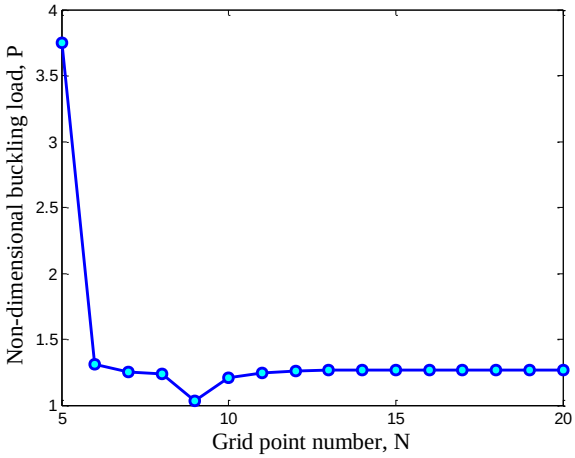

Fig. 2 Accuracy and convergence of DQM

Table 3 Critical buckling loadof laminated sandwich conical shell for ϕ = 15°

Mode	Zhong and Reimerdes (2007)	NASTRAN (2007)	Present work
1	-1.718e6 N	-1.734e6 N	-1.724e6 N
2	----	----	-3.301e6 N

a sandwich conical shell with a vertex half-angle of ϕ = 15° and the geometrical and material properties the same as Zhong and Reimerdes (2007), is investigated. Based on DQM, the critical buckling load is calculated and compared with Zhong and Reimerdes (2007) in Table 3. The results show the accuracy of this work.

7.3 The influence of parameters

Figs. 3-10, show the influences of different parameters on the non-dimensional buckling load versus weight percent of CNTs. In all of the figures, with enhancing the CNTs weight percent, the non-dimensional buckling load is enhanced up to 60% due to improve in the stiffness of the sandwich structure.

Thenon-dimensional buckling load is plotted versus the weight percent of CNTs for different non-dimensional external applied voltage $(V^* = (V_0/L)\sqrt{E^M/\in_{11}})$ to top layer of the sandwich structure. The results show that applying positive and negative external voltage, respectively leads to decrease and increase in the non-dimensional buckling load of the structure. It is due to this fact that applying positive and negative external voltage induces tensile and compressive loads in the structure, respectively. In addition, with enhancing the CNTs weight percent, the effects of external voltage become more prominent. In other words, comparing to external voltage equal to zero, applying negative external voltage increases about 11% the buckling load of the sandwich structure.

The effects of moisture and temperature changes on the non-dimensional buckling load versus the weight percent of CNTs are shown in Figs. 4 and 5, respectively. It is obvious that with enhancing the moisture and temperature changes, the non-dimensional buckling load is reduced. It

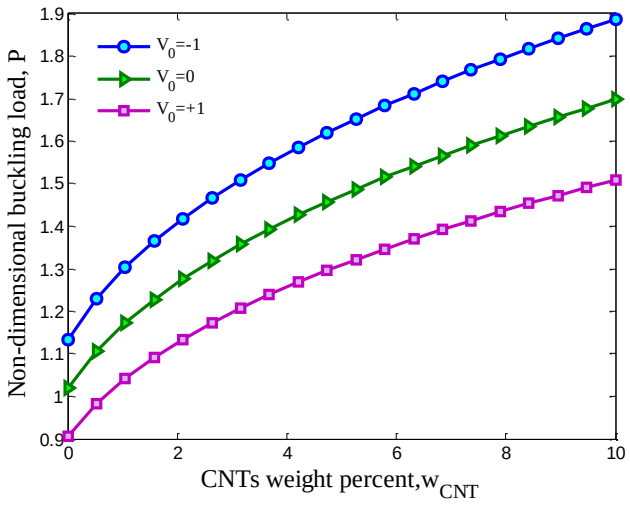

Fig. 3 The influence of external voltage on the non-dimensional buckling load of the structure versus weight percent of CNTs

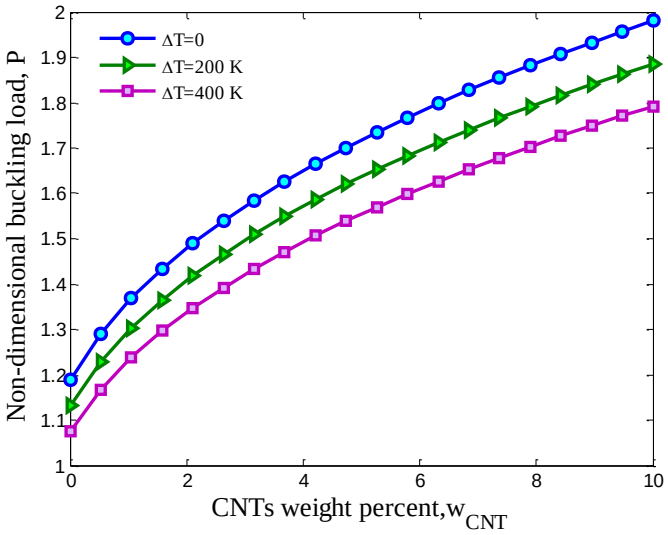

Fig. 4 The influence of temperature change on the non-dimensional buckling load of the structure versus weight percent of CNTs

is since the stiffness of the sandwich structure will be reduced. In conclusion, applying the moisture and temperature changes to the structure decreases the non-dimensional buckling load.

Fig. 6 illustrates the effect of different boundary conditions on the non-dimensional buckling load as a function of weight percent of CNTs. This figure shows the considerable effect of boundary condition on the buckling load of the smart sandwich structure. As can be seen, the non-dimensional buckling load of the sandwich truncated conical shell with CC boundary condition is

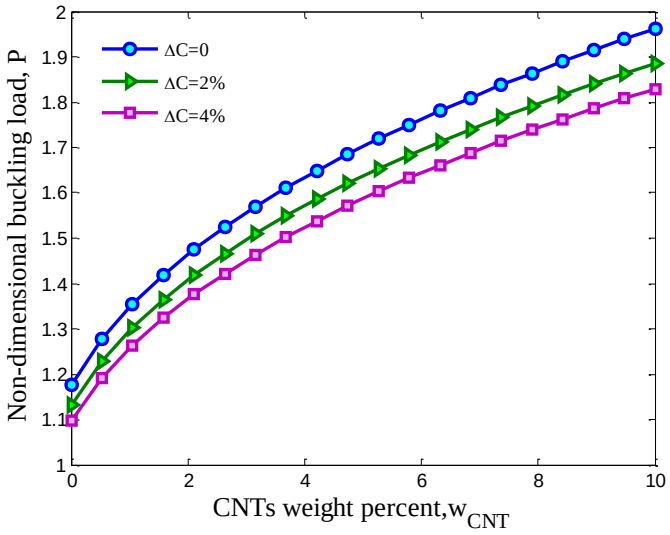

Fig. 5 The influence of moisture change on the non-dimensional buckling load of the structure versus weight percent of CNTs

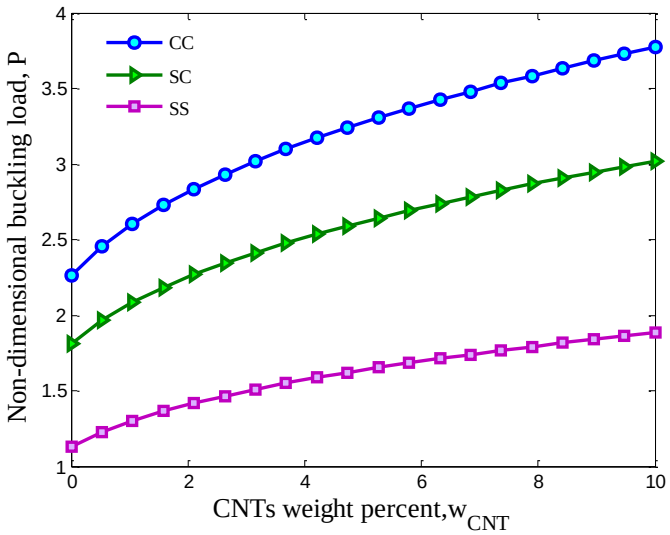

Fig. 6 The influence of boundary conditions on the non-dimensional buckling load of the structure versus weight percent of CNTs

about 24% and 2 times higher than that with CS and SS one. In addition, the non-dimensional buckling load for the sandwich truncated conical shell with CS boundary condition is about 60% higher than that of SS ones. It is due to this fact that the clamped boundary condition improves the rigidity of the structure and hence the buckling load increases.

Fig. 7 demonstrates the influence of cone length to large radius ratio on the non-dimensional buckling load versus the weight percent of CNTs. It is found that increasing the cone length to

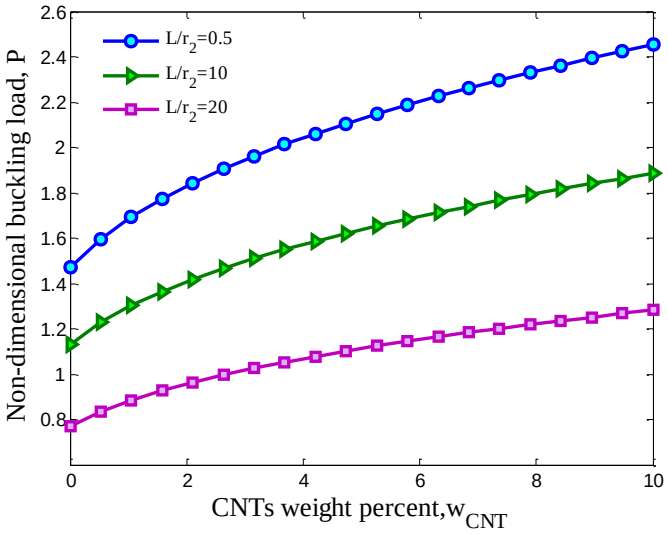

Fig. 7 The influence of cone length to large radius ratio on the non-dimensional buckling load of the structure versus weight percent of CNTs

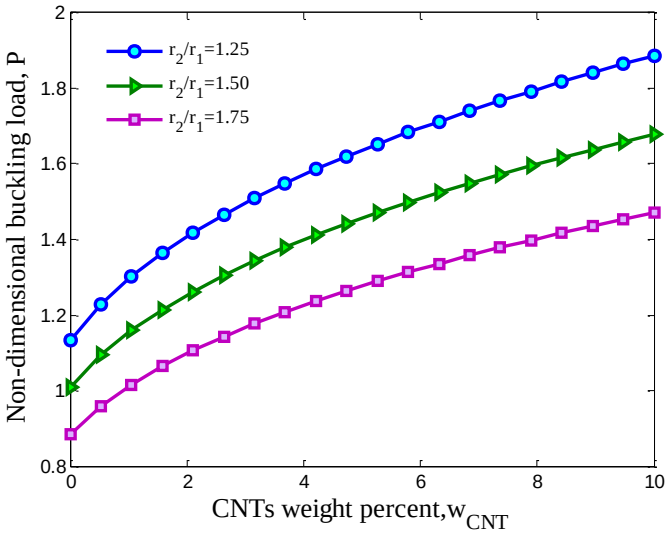

Fig. 8 The influence of cone large radius to small radius of the cone on the non-dimensional buckling load of the structure versus weight percent of CNTs

large radius ratio leads to reduction in the non-dimensional buckling load. This is since with enhancing the cone length to large radius ratio, the structure stiffness reduces. It is also found that with enhancing the cone length to large radius ratio, the effect of CNTs weight percent on the non-dimensional buckling load decreases and the changes of buckling load versus the weight percent of CNTs become more linear. This physically due to this reason that with enhancing the cone length to large radius ratio, the shear effects gets less and stiffness of system decreases. The influence of large radius to small radius of the cone on the non-dimensional buckling load versus the weight

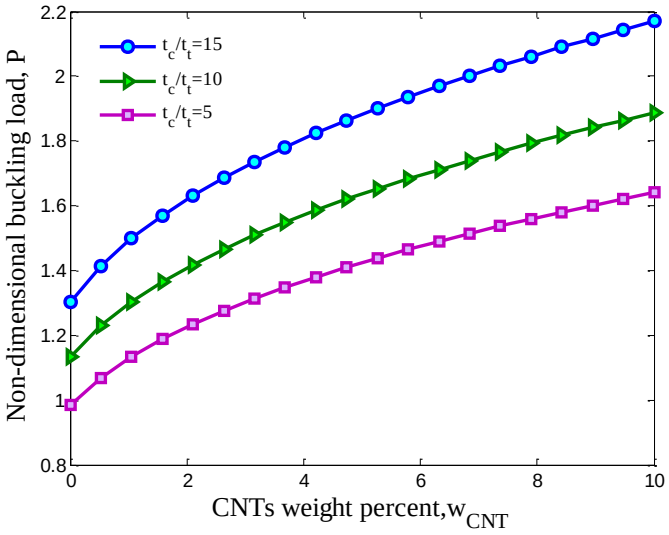

Fig. 9 The influence of core thickness to face sheets thickness on the non-dimensional buckling load of the structure versus weight percent of CNTs

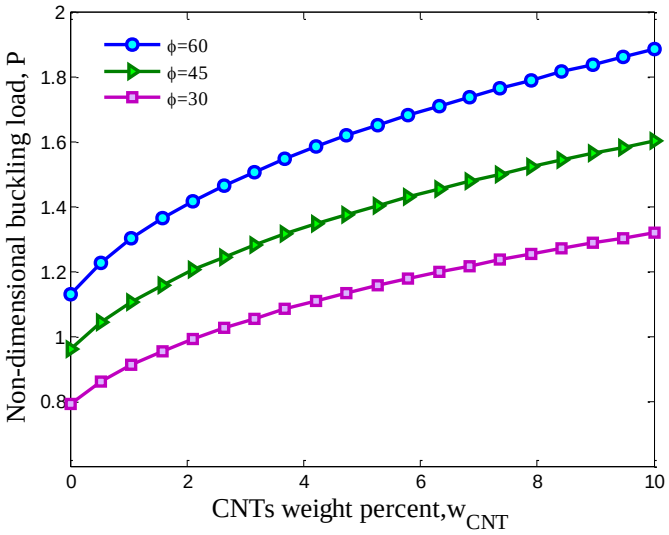

Fig. 10 The influence of cone semi vertex angle on the non-dimensional buckling load of the structure versus weight percent of CNTs

percent of CNTs is shown in Fig. 8. It can be concluded that, with enhancing the large radius to small radius of the cone, the non-dimensional buckling load is reduced due to decrease in the rigidity and stiffness of the sandwich structure.

Fig. 9 presents the influence of the core thickness to face sheets thickness ratio on the non-dimensional buckling load versus weight percent of CNTs. The results show that with enhancing the core thickness to face sheets thickness, the non-dimensional buckling load is increased due to improve in the structure stiffness.

Fig. 10 demonstrates the influence of semi vertex angle of the cone on the non-dimensional buckling load versus the weight percent of CNTs. It can be observed that the non-dimensional buckling load enhances with increasing the semi vertex angle of the cone from 30 to 60 degree.

8. Conclusions

Buckling response of truncated nanocomposite conical shell integrated with piezoelectric layers was presented in this article. The core was reinforced by CNTs and carbon fibers where the Halpin-Tsai model was applied for obtaining the equivalent material properties. The piezoelectric layers were subjected to 3D electric field and the sandwich structure was in hygrothermal environment. Using layerwise FSDT, the governing equations were calculated and solved by DQM in order to calculate the buckling load. The influences of some parameters such as boundary conditions, CNTs weight percent, cone semi vertex angle, geometrical parameters, moisture and temperature changes and external voltage were investigated on the buckling load of the smart structure. The results show that imposing negative voltage enhances the non-dimensional buckling load comparing to external voltage equal to zero about 11%. With enhancing the moisture and temperature changes, the non-dimensional buckling load will be decreased. Furthermore, with enhancing the CNTs weight percent, the non-dimensional buckling load was increased about 60%. Meanwhile, the non-dimensional buckling load of the CC structure is about 24% and 2 times higher than that with CS and SS one. In addition, enhancing the cone length to large radius ratio and cone large to small radius leads to reduction in the non-dimensional buckling load.

References

Abediokhchi, J., Kouchakzadeh, M.A. and Shakouri, M. (2013), "Buckling analysis of cross-ply laminated conical panels using GDQ method", *Compos. Part B: Eng.*, **55**, 440-446.

Ahouel, M., Houari, M.S.A., Adda Bedia, E.A. and Tounsi, A. (2016), "Size-dependent mechanical behavior of functionally graded trigonometric shear deformable nanobeams including neutral surface position concept", *Steel Compos. Struct., Int. J.*, **20**(5), 963-981.

Araújo, A.L, Carvalho, V.S., MotaSoares, C.M., Belinha, J. and Ferreira, A.J.M. (2016), "Vibration analysis of laminated soft core sandwich iplates with piezoelectric sensors and actuators", *Compos. Struct.*, **151**, 91-98.

Attia, A., Tounsi, A., Adda Bedia, E.A. and Mahmoud, S.R. (2015), "Free vibration analysis of functionally graded plates with temperature-dependent properties using various four variable refined plate theories", *Steel Compos. Struct., Int. J.*, **18**(1), 187-212.

Aylikci, F., Akbarov, S.D. and Yahnioglu, N. (2017), "Buckling delamination of a PZT/Metal/PZT sandwich rectangular thick plate containing interface inner band cracks", *Compos. Struct.*, **202**, 9-16.

Chikh, A., Tounsi, A., Hebali, H. and Mahmoud, S.R. (2017), "Thermal buckling analysis of cross-ply laminated plates using a simplified HSDT", *Smart Struct. Syst., Int. J.*, **19**(3), 289-297.

Demir, Ç., Mercan, K. and Civalek, Ö. (2016), "Determination of critical buckling loads of isotropic, FGM and laminated truncated conical panel", *Compos. Part B: Eng.*, **94**, 1-10.

Duc, N.D., Hadavinia, H., Van Thu, P. and Quan, T.Q. (2015), "Vibration and nonlinear dynamic response of imperfect three-phase polymer nanocomposite panel resting on elastic foundations under hydrodynamic loads", *Compos. Struct.*, **131**, 229-237.

Duc, N.D., Cong, P.H., Tuan, N.D., Tran, P. and Van Thanh, N. (2017a), "Thermal and mechanical stability of functionally graded carbon nanotubes (FG CNT)-reinforced composite truncated conical shells

surrounded by the elastic foundation", *Thin-Wall. Struct.*, **115**, 300-310.
Duc, N.D., Lee, J., Nguyen-Thoi, T. and Thang, P.T. (2017b), "Static response and free vibration of functionally graded carbon nanotube-reinforced composite rectangular plates resting on Winkler-Pasternak elastic foundations", *Aerosp. Sci. Technol.*, **68**, 391-402.
Duc, N.D., Tran, Q.Q. and Nguyen, D.K. (2017c), "New approach to investigate nonlinear dynamic response and vibration of imperfect functionally graded carbon nanotube reinforced composite double curved shallow shells subjected to blast load and temperature", *Aerosp. Sci. Technol.*, **71**, 360-372.
Duc, N.D., Seung-Eock, K., Quan, T.Q., Long, D.D. and Anh, V.M. (2018), "Nonlinear dynamic response and vibration of nanocomposite multilayer organic solar cell", *Compos. Struct.*, **184**, 1137-1144.
Ebrahimi, F. and Barati, M.R. (2018), "Stability analysis of functionally graded heterogeneous piezoelectric nanobeams based on nonlocal elasticity theory", *Adv. Nano Res., Int. J.*, **6**, 93-112.
Ebrahimi, F. and Jafari, A. (2017), "Investigating vibration behavior of smart imperfect functionally graded beam subjected to magnetic-electric fields based on refined shear deformation theory", *Adv. Nano Res., Int. J.*, **5**(4), 281-301.
El-Haina, F., Bakora, A., Bousahla, A.A. and Hassan, S. (2017), "A simple analytical approach for thermal buckling of thick functionally graded sandwich plates", *Struct. Eng. Mech., Int. J.*, **63**(5), 585-595.
Hajmohammad, M.H., Zarei, M.S., Nouri, A. and Kolahchi, R. (2017a), "Dynamic buckling of sensor/ functionally graded-carbon nanotubes reinforced laminated plates/actuator based on sinusoidal-viscopiezoelasticity theories", *J. Sandw. Struct. Mater.*, 1099636217720373.
Hajmohammad, M.H., Azizkhani, M.B. and Kolahchi, R. (2017b), "Multiphase nanocomposite viscoelastic laminated conical shells subjected to magneto-hygrothermal loads: Dynamic buckling analysis", *Int. J. Mech. Sci.*, **137**, 205-213.
Hull, D. and Clyne, T. (2001), *An Introduction to Composite Materials*, Cambridge University Press.
Kapuria, S., Dumir, P.C. and Ahmed, A. (2003), "An efficient coupled layerwise theory for static analysis of piezoelectric sandwich beams", *Arch. Appl. Mech.*, **73**, 147-159.
Karami, B., Shahsavari, D., Li, L., Karami, M. and Janghorban, M. (2018), "Thermal buckling of embedded sandwich piezoelectric nanoplates with functionally graded core by a nonlocal second-order shear deformation theory" *Proceed. Inst. Mech. Eng., Part C: J. Mech. Eng. Sci.*, 0954406218756451.
Khan, A.H. and Patel, B.P. (2015), "On the nonlinear dynamics of bimodular laminated composite conical panels", *Nonlinear Dyn.*, **79**, 1495-1509.
Khetir, H., Bouiadjra, M.B., Houari, M.S.A., Tounsi, A. and Mahmoud, S.R. (2017), "A new nonlocal trigonometric shear deformation theory for thermal buckling analysis of embedded nanosize FG plates", *Struct. Eng. Mech., Int. J.*, **64**(4), 391-402.
Kolahchi, R. (2017), "A comparative study on the bending, vibration and buckling of viscoelastic sandwich nano-plates based on different nonlocal theoriesusing DC, HDQ and DQ methods", *Aerosp. Sci. Technol.*, **66**, 235-248.
Kolahchi, R., Hosseini, H. and Esmailpour, M. (2016a), "Differential cubature and quadrature-Bolotin methods for dynamic stability of embedded piezoelectric nanoplates based onvisco-nonlocal-piezoelasticity theories", *Compos. Struct.*, **157**, 174-186.
Kolahchi, R., Zarei, M.S. and Esmailpour, M. (2016b), "Dynamic stability analysis of temperature-dependent functionally graded CNT-reinforced visco-plates resting on orthotropic elastomeric medium", *Compos. Struct.*, **150**, 255-265.
Kolahchi, R., Zarei, M.S., Hajmohammad, M.H. and Nouri, A. (2017a), "Wave propagation of embedded viscoelastic FG-CNT-reinforced sandwich plates integrated with sensor and actuator based on refined Zigzag theory", *Int. J. Mech. Sci.*, **130**, 534-545.
Kolahchi, R., Keshtegar, B. and Fakhar, M.H. (2017b), "Optimization of dynamic buckling for sandwich nanocomposite plates with sensor and actuator layer based on sinusoidal visco-piezoelasticity theories using Grey Wolf algorithm", *J. Sandw. Struct. Mater.*, 1099636217731071.
Larbi Chaht, F., Kaci, A., Houari, M.S.A. and Hassan, S. (2015), "Bending and buckling analyses of functionally graded material (FGM) size-dependent nanoscale beams including the thickness stretching effect", *Steel Compos. Struct., Int. J.*, **18**(2), 425-442.

Mahi, A., Bedia, E.A.A. and Tounsi, A. (2015), "A new hyperbolic shear deformation theory for bending and free vibration analysis of isotropic, functionally graded, sandwich and laminated composite plates", *Appl. Math. Model.*, **39**, 2489-2508.

Malekzade Fard, K. and Livani, M. (2014), "The buckling of truncated conical sandwich panels under axial compression and external pressur", *Proceed. Inst. Mech. Eng., Part C: J. Mech. Eng. Sci.*, **229**, 1965-1978.

Mehri, M., Asadi, H. and Wang, Q. (2016), "Buckling and vibration analysis of a pressurized CNT reinforced functionally graded truncated conical shell under an axial compression using HDQ method", *Comput. Meth. Appl. Mech. Eng.*, **303**, 75-100.

Menasria, A., Bouhadra, A., Tounsi, A. and Hassan, S. (2017), "A new and simple HSDT for thermal stability analysis of FG sandwich plates", *Steel Compos. Struct., Int. J.*, **25**(2), 157-175.

Meziane, M.A.A., Abdelaziz, H.H. and Tounsi, A.T. (2014), "An efficient and simple refined theory for buckling and free vibration of exponentially graded sandwich plates under various boundary conditions", *J. Sandw. Struct. Mater.*, **16**(3), 293-318.

Mouffoki, A., Adda Bedia, E.A., Houari, M.S.A. and Hassan, S. (2017), "Vibration analysis of nonlocal advanced nanobeams in hygro-thermal environment using a new two-unknown trigonometric shear deformation beam theory", *Smart Struct. Syst., Int. J.*, **20**(3), 369-383.

Nasihatgozar, M. and Khalili, S.M.R. (2017), "Vibration and buckling analysis of laminated sandwich conical shells using higher order shear deformation theory and differential quadrature method", *J. Sandw. Struct. Mater.*, 1099636217715806.

Tong, L. (1994), "Free vibration of laminated conical shells including transverse shear deformation", *Int. J. Solid Struct.*, **31**, 443-456.

Plagianakos, Th.S. and Papadopoulos, E.G. (2015), "Coupled higher-order layerwise mechanics and finite element for cylindrical composite and sandwich shells with piezoelectric transducers", *Eur. J. Mech. - A/Solids*, **54**, 11-23.

Reddy, J. (2003), *Mechanics of Laminated Composite Plates and Shells, Theory and Application*, CRC Press, Boca Raton, FL, USA.

Sharnappa, S., Ganesan, N. and Sethuraman, R. (2007), "Free Vibration Analysis Of Truncated Sandwich Conical Shells With Constrained Electro-Rheological Fluid Damping", *Vibration Problems ICOVP*, **1**, 357-364.

Shekari, A., Ashenai Ghasemi, F. and Malekzadehfard, K. (2017), "Free Damped Vibration of Rotating Truncated Conical Sandwich Shells Using an Improved High-Order Theory", *Lat. Am. J. Solids Struct.*, **14**(12), 2291-2323.

Sofiyev, A.H., Osmancelebioglu, E. and Osmancelebioglu, A. (2017), "The free vibration of sandwich truncated conical shells containing functionally graded layers within the shear deformation theory", *Compos. Part B: Eng.*, **120**, 197-211.

Thanh, N.V., Khoa, N.D., Tuan, N.D., Tran, P. and Duc, N.D. (2017), "Nonlinear dynamic response and vibration of functionally graded carbon nanotube-reinforced composite (FG-CNTRC) shear deformable plates with temperature-dependent material properties", *J. Therm. Stres.*, **40**, 1254-1274.

Viswanathan, K.K., Lee, J.H., Aziz, Z.A., Hossain, I., Rongqiao, H.W. and Abdullah, H.Y. (2012), "Vibration analysis of cross-ply laminated truncated conical shells using a spline method", *J. Eng. Math.*, **76**, 139-156.

Viswanathan, K.K., Saira, J., Kandasamy, P., Aziz, Z.A. and Abu Bakar, I. (2015), "Free vibration of anti-symmetric angle-ply laminated conical shells", *Compos. Struct.*, **122**, 488-495.

Zarei, M.S., Kolahchi, R., Hajmohammad, M.H. and Maleki, M. (2017), "Seismic response of under water fluid-conveying concrete pipes reinforced with SiO_2 nanoparticles and fiber reinforced polymer (FRP) layer", *Soil Dyn. Earth. Eng.*, **103**, 76-85.

Zemri, A., Houari, M.S.A., Bousahla, A.A. and Tounsi, A. (2015), "A mechanical response of functionally graded nanoscale beam: an assessment of a refined nonlocal shear deformation theory beam theory", *Struct. Eng. Mech., Int. J.*, **54**(4), 693-710.

Zidi, M., Tounsi, A. and Bég, O.A. (2014), "Bending analysis of FGM plates under hygro-thermo-mechanical loading using a four variable refined plate theory", *Aerosp. Sci. Tech.*, **34**, 24-34.

Zhong, C. and Reimerdes, H.G. (2007), "Stability behavior of cylindrical and conical sandwich shells with flexible core", *J. Sandw. Struct. Mater.*, **9**(2), 143-166.

JL